communications biology

Article

https://doi.org/10.1038/s42003-024-07173-7

# Iterative crRNA design and a PAM-free strategy enabled an ultra-specific RPA-CRISPR/Cas12a detection platform



Xujian Mao[1,4] ✉, Jian Xu[1,4], Jingyi Jiang[1,4], Qiong Li[1], Ping Yao[1], Jinyi Jiang[1], Li Gong[1], Yin Dong[1], Bowen Tu[1], Rong Wang[3], Hongbing Tang[1] ✉, Fang Yao[1,2,3] ✉ & Fengming Wang[1,3] ✉

CRISPR/Cas12a is a highly promising detection tool. However, detecting single nucleotide variations (SNVs) remains challenging. Here, we elucidate Cas12a specificity through crRNA engineering and profiling of single- and double-base mismatch tolerance across three targets. Our findings indicate that Cas12a specificity depends on the number, type, location, and distance of mismatches within the R-loop. We also find that introducing a wobble base pair at position 14 of the R-loop does not affect the free energy change when the spacer length is truncated to 17 bp. Therefore, we develop a new universal specificity enhancement strategy via iterative crRNA design, involving truncated spacers and a wobble base pair at position 14 of the R-loop, which tremendously increases specificity without sacrificing sensitivity. Additionally, we construct a PAM-free one-pot detection platform for SARS-CoV-2 variants, which effectively distinguishes SNV targets across various GC contents. In summary, our work reveals new insights into the specificity mechanism of Cas12a and demonstrates significant potential for in vitro diagnostics.

In recent years, the CRISPR/Cas system, which is derived from the adaptive immune mechanism of prokaryotes and is characterized by high developability, simplicity, and efficiency, has led to revolutionary breakthroughs in vivo gene editing technology and has been applied in vitro diagnosis[1,2]. The CRISPR-associated proteins Cas9 and Cas12a are two of the most influential and widely used members of the Cas family. They can bind to the protospacer-adjacent motif (PAM) in the genome to cause the local opening of the double-stranded DNA (dsDNA) target, allowing Watson–Crick base pairing between the guide RNA (gRNA) and the template strand (TS) of the dsDNA target. Finally, the R-loop structure is formed, which triggers the structural rearrangement of the Cas nuclease domain to activate its cis-cleavage activity, creating dsDNA breaks for the purpose of gene editing[3–8].

Unlike Cas9, Cas12a requires only a single CRISPR RNA (crRNA) as a gRNA and does not require tracrRNA[3]; Cas12a can also recognize single-stranded DNA (ssDNA) targets and perform cleavage with no PAM[6,9]. In addition, after the target is loaded, the CRISPR/Cas12a system can perform nonspecific trans-cleavage of nearby ssDNA molecules[6]. Based on this characteristic, ssDNA with a fluorescent reporter group and quenching group was introduced as a reporter probe molecule. When the target DNA forms an R-loop structure with crRNA to activate Cas12a, the reporter probe molecule is cleaved, and the fluorescence signal is released. This behavior has applications in the field of nucleic acid detection and biosensors[10]. To achieve highly sensitive molecular detection, it is usually necessary to combine target nucleic acid preamplification technology with CRISPR detection technology. The combination of CRISPR/Cas12a and recombinase polymerase amplification (RPA) can achieve the amplification and detection of nucleic acids at a constant temperature of 37°C, which is highly valuable for the development of simple nucleic acid detection methods and instruments. Several CRISPR/Cas12a-based diagnostic techniques, such as DETECTR and HOLMES, have been developed[9,11].

The detection of single nucleotide variations (SNVs) is highly important for diagnosing genetic diseases, cancer, and pathogen variants. However, the specificity of Cas12a is controversial, although the cis-cleavage activity of Cas12a has been reported to be greater than that of Cas9 both in vivo and in vitro, especially in the PAM-proximal region[12,13]. However, there is substantial evidence that Cas12a cis-cleavage not only has a high tolerance to a single mismatch but also can tolerate multiple mismatches[14,15]. The trans-cleavage specificity of Cas12a is also poor. For these reasons, Cas12a cannot distinguish SNVs[15–17]. In general, the specificity of Cas12a is unsatisfactory. The signal-to-noise ratio between wild-type and mutant sequences is very low or even absent, which does not meet the requirements for SNV diagnosis and is thus a bottleneck for application.

[1]Pathogen Inspection Center, Changzhou Center for Disease Control and Prevention, Changzhou, Jiangsu, China. [2]Changzhou Institute for Advanced Study of Public Health, Nanjing Medical University, Changzhou, Jiangsu, China. [3]China School of Public Health, Nanjing Medical University, Nanjing, Jiangsu, China. [4]These authors contributed equally: Xujian Mao, Jian Xu, Jingyi Jiang. ✉e-mail: m5575383@163.com; 466167580@qq.com; 2366150165@qq.com; wfm0519@163.com

The specificity of the CRISPR/Cas12a system can be increased mainly by modifying the Cas12a enzyme or crRNA sequence[18–20]. Compared with the cumbersome modification and screening of Cas enzymes, crRNA sequence modification is a simpler strategy[21,22]. At present, crRNA is modified mainly by the following methods: ① chemical modification of part of the crRNA sequence[23]; ② truncation of crRNA length[24,25]; ③ alteration of the crRNA secondary structure[22]; ④ replacement of part of the crRNA sequence with DNA bases[16,26]; ⑤ introduction of additional mismatched bases into the crRNA[27–31]; ⑥ and the insertion or deletion of bases in the crRNA-target pairing region to form DNA–RNA bubbles[32].

Although there are several ways to improve the specificity of the CRISPR/Cas12a system by modifying crRNA, there are still some deficiencies. ①The specificity increase is not significant, and the signal-to-noise ratio between the mutant and wild type for certain targets is less than 5-fold[11,16,23]. ②There is a trade-off between sensitivity and specificity. Although chemically modified gRNAs exhibit increased specificity, their cis-cleavage activity is somewhat attenuated for certain targets[33,34]. ③The applicability is limited rather than universal, as different targets require chemical modification of their crRNAs at different locations[34], and the optimal site for introducing additional mismatched bases varies among different targets[31,35]. Therefore, the specificity of CRISPR/Cas12a SNV detection technology needs to be dramatically improved while maintaining its sensitivity and expanding its universality.

In this study, we first modified the sequences of various regions of crRNA and discovered that truncating the spacer region is the most efficient method for enhancing the specificity of Cas12a trans-cleavage while preserving its sensitivity. Notably, through the step-by-step shortening of three targets by a single bp, 17 bp was shown to be the shortest spacer length at which sensitivity is generally not lost. Moreover, for a spacer length of 17 bp, the introduction of wobble base pairing at R-loop position 14 to form double mismatch versus single mismatch strategy also improved specificity without decreasing sensitivity. Furthermore, we introduced the PAM sequence into the RPA primer, overcoming the limitations of PAM by avoiding the position requirement of wobble base pair. Moreover, the addition of glycerol enabled a one-pot procedure, preventing aerosol contamination and increasing the ease of operation, which can expand the applicability.

In summary, we developed a simple and highly specific SNV detection strategy while maintaining sensitivity and universality through the iterative modification of crRNA. We also provided a mechanistic framework to explain the underlying principle. Additionally, a PAM-free one-pot SNV detection scheme was established and applied to the detection of SARS-CoV-2 variants.

## CrRNA modification affects the specificity and sensitivity of the CRISPR/Cas12a reaction

CrRNA is an RNA molecule with a defined secondary structure. The 5′ end contains the scaffold sequence necessary for Cas12a binding, which includes scaffold, stem, and loop sequences, and the 3′ end contains a spacer sequence complementary to a 20 bp target (Supplementary Fig. 1). The stem, loop, scaffold, and spacer of crRNA in the secondary structure interact with Cas12a, exerting variable effects on the formation kinetics of the R-loop[3,36]. We selected the *CPSIT*_0429 gene (specific for *Chlamydia psittaci* detection[37]) as a target, constructed 34 different modifications in different regions of its crRNA, including the spacer, scaffold, loop, stem, and extension regions, and preliminarily determined the effects on the trans-cleavage activity of Cas12a (Fig. 1a and Supplementary Data 1). For each crRNA modification region, we selected 1 or 2 mutants that showed either a slight decrease or no significant change in trans-cleavage activity compared to the wild type, for a total of seven crRNA mutants chosen for further experiments. Through analytical sensitivity experiments, we found that the M65 modification was consistent with the wild type and that other modifications had varying effects on the limit of detection (Supplementary Fig. 2). The mismatch tolerance of these modifications was subsequently evaluated by A-G and T-C mutations of a single base or two adjacent bases in the target (Fig. 1b and Supplementary Fig. 3a). Four modifications significantly increased the specificity: M39 (scaffold engineering: 3′ truncation 1 bp); M42 + M43 (loop engineering: 3′ split); M63 (extension engineering: 3′ foldback blocking 15 bp); M65 (spacer engineering: 3′ truncation 2 bp). Combined with the results of analytical sensitivity experiments, these findings show that M65 modification can improve detection specificity without decreasing sensitivity.

The results of single-base mutation showed that increasing specificity by crRNA modification was position dependent and nonsignificant (Fig. 1b and Supplementary Fig. 3a). The signal-to-noise ratio between the wild-type and mutant sequences in both PAM-proximal and PAM-distal regions was low, while it was higher at positions 12 and 13 relative to the PAM. The M65 modification had the best signal-to-noise ratio between the wild-type and mutant sequences at position 12 relative to the PAM, but only by a factor of 10. Compared with that of single-base mutations, the mismatch tolerance of adjacent double-base mutations decreased sharply, especially for mut27, mut31, mut32, mut35, mut36, and mut37 (Fig. 1b and Supplementary Fig. 3a). A previous study also showed that adjacent mismatches strongly affect the formation of the R-loop[38]. These findings suggested that introducing 'double mismatch versus single mismatch strategy' might further improve the detection specificity. That is, a single-base mutation is pre-introduced adjacent to the position in the spacer sequence that matches a single-base mutation site in the target sequence, and thus, when the crRNA binds to the target sequence and a single-base mutation, an adjacent double-base mismatch is generated in the R-loop. With this strategy, the signal-to-noise ratio between the wild-type and mutant sequences of the four elevated-specificity crRNA modifications increased significantly, with many modifications achieving increases exceeding 10-fold (Fig. 1c). The M65 modification was the most obvious, but there were still many positions with insufficiently increased specificity. In summary, the introduction of double mismatch versus single mismatch strategy can further increase the detection specificity of crRNA modification, but this effect is position dependent.

## Further characterization of truncated spacer with three targets

To further analyse the effect of spacer truncation on specificity and universality for different targets, we added two additional targets, D614G and R346T (SARS-CoV-2 point mutation targets). As in the case of the *CPSIT*_0429 target, we shortened the spacer length from 20 bp to 15 bp, reducing it by 1 bp each time. When the spacer was truncated to 17 bp, there was no significant decrease in the detection signal for the three targets, and their detection limits were consistent with those at 20 bp (Supplementary Figs. 2h and 4). However, when the spacer was truncated to 16 bp, there was a significant difference in the detection signal for different targets. The D614G and R346T targets still had strong signals, while the signal of the *CPSIT*_0429 target decreased sharply. These observations highlight the inconsistent effects of 16 bp truncated crRNAs across different targets, suggesting the presence of target-specific factors that influence signal strength and require further exploration. There was no apparent signal for any of the three targets when the spacer was truncated to 15 bp (Fig. 2a and Supplementary Fig. 5).

Single-base mutations at three target sites showed that the increase in specificity upon spacer truncation was dependent on the number of truncations. As the number of spacer truncations increases, the tolerance for base mismatches also decreases (Fig. 2b and Supplementary Fig. 5). A 17 bp spacer ensured the balance point of R-loop stability (without reducing sensitivity) and maximally enhanced specificity. Shortening the spacer to 17 bp resulted in position-dependent[39] and nonsignificant increases in specificity. The signal-to-noise ratio between the wild-type and mutant strains in the PAM-proximal and PAM-distal regions was relatively low but was more pronounced in the middle region of the spacer. For the R346T target alone, the signal-to-noise ratio between the wild-type and mutant strains at positions 10 and 15 relative to the PAM was more than 10 times greater. Notably, this effect also has target specificity. For example, at position 12 relative to the PAM, the signal-to-noise ratio of the *CPSIT*_0429 target was significantly improved by approximately 10-fold;

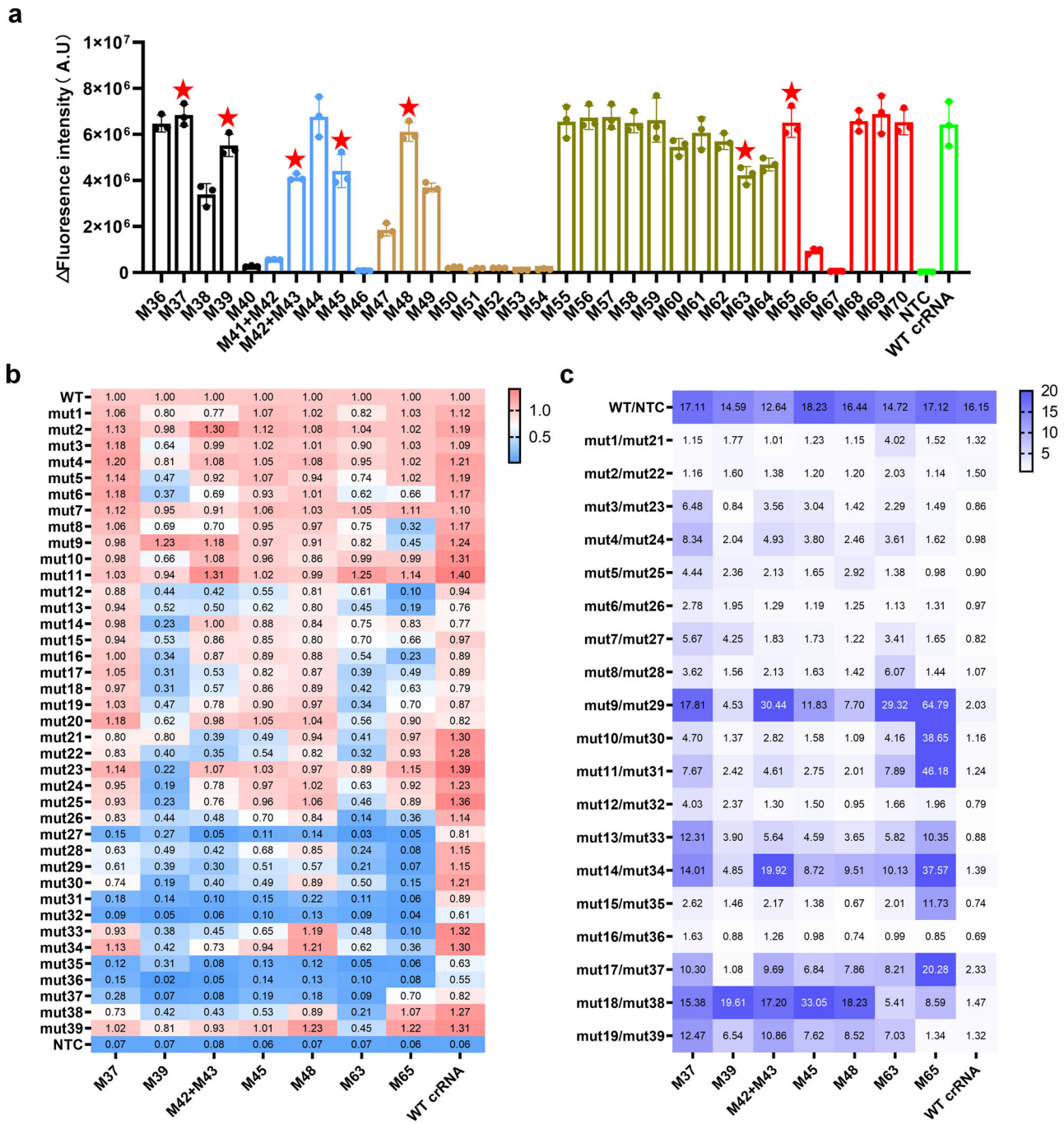


**Fig. 1 | The specificity of different crRNA modifications. a** Depiction of the trans-cleavage activity of crRNA modifications. The fluorescence value increase within 1 h for 34 different crRNA modifications or an unmodified crRNA (WT crRNA) in the presence of the *CPSIT*_0429 activator. CrRNA modifications in the same region are shown in the same color. A red star (★) indicates the crRNA mutants that were selected for further experiments. **b** The mismatch tolerance of various crRNAs to matched or mismatched *CPSIT*_0429 activators was evaluated. Mut1-20 and mut21-39 contained one mismatch and two adjacent mismatches relative to the on-target site, respectively. All sequences are provided in Supplementary Data 2, 3. Heatmap indicating the mean fold change in fluorescence value within 1 h for the mutant activators normalized to that of the corresponding wild-type activator. The values in the heatmap represent the inverse multiples of specificity. **c** The mismatch tolerance of various crRNAs to mismatched *CPSIT*_0429 activators with the double mismatch versus single mismatch strategy was evaluated. Heatmap indicating the mean fold change in fluorescence value within 1 h for the single mismatch activator normalized to that of the corresponding adjacent double mismatch activator. The values in the heatmap represent the multiples of specificity.

the improvement in the D614G target was moderate, only approximately 2-fold; and that of the R346T target was close to 1, indicating almost no significant improvement. In summary, increasing the specificity by truncating the spacer to 17 bp has inconsistent effects on different targets and different positions. Therefore, its universality and single-base discrimination ability still need to be improved.

Compared to single-base recognition, adjacent double-base mismatch recognition is more effectively improved when the spacer is shortened (Fig. 2b and Supplementary Fig. 5). After introducing the double mismatch versus single mismatch strategy, the specificity of the three targets significantly increased only when the spacer was truncated to 18 bp and 17 bp (Fig. 2c). This specificity increase was also position dependent and target

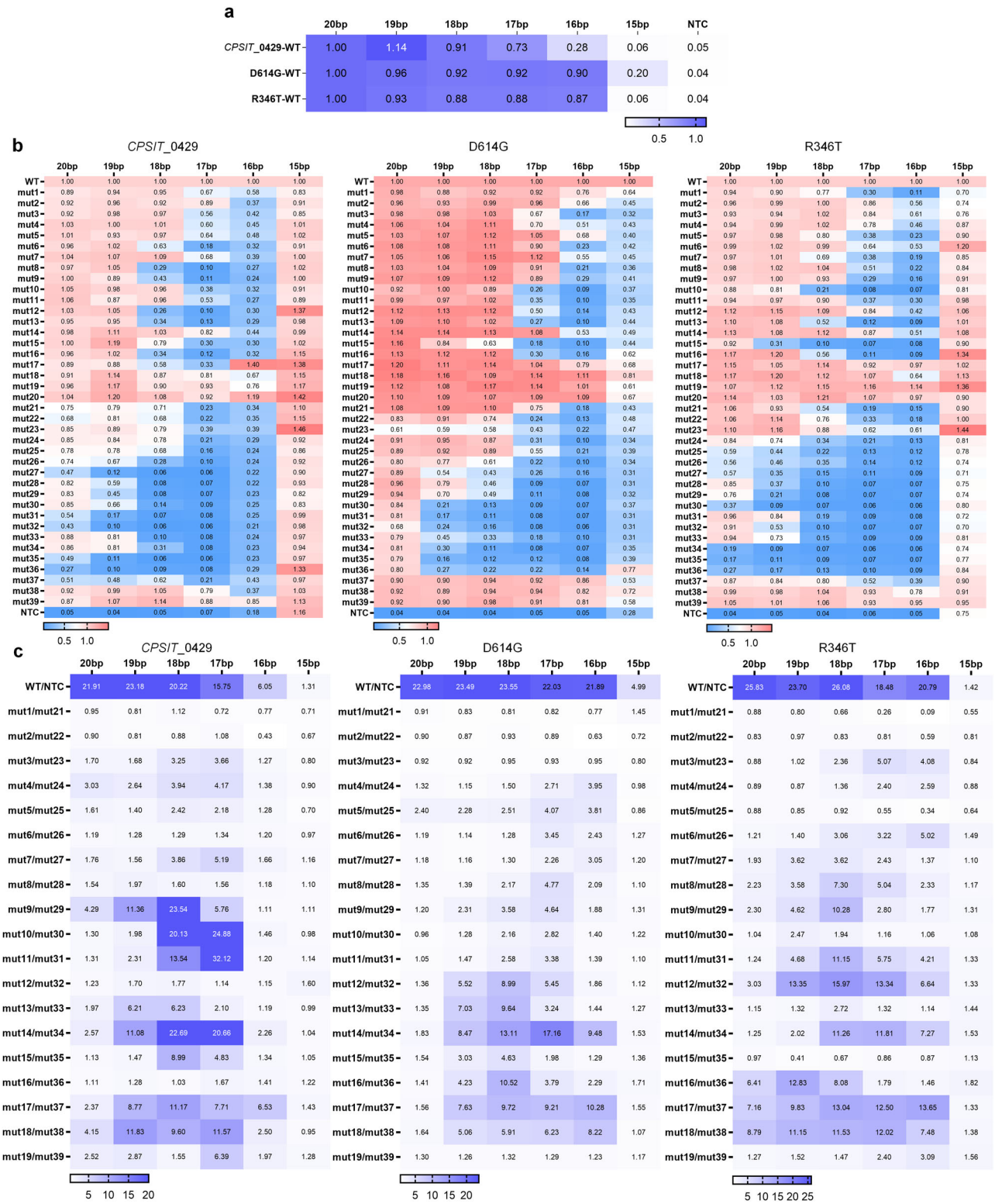


**Fig. 2 | The specificity of truncated spacer for three targets. a** Heatmap indicating the trans-cleavage activity on the three targets tested in the presence of crRNAs with different spacer lengths (20-15 bp). The values in the heatmap represent the mean fluorescence value increase within 1 h for truncated crRNA normalized to that of the corresponding unmodified crRNA. NTC, non-target control. **b** Evaluate the mismatch tolerance of various crRNAs with different spacer lengths to matched or mismatched activators of the *CPSIT*_0429, D614G, and R346T targets. All the sequences are provided in Supplementary Data 2, 3. Heatmap indicating the mean fold change in fluorescence value within 1 h for the mutated activators normalized to that of the corresponding wild-type activator. **c** The mismatch tolerance of various crRNAs to mismatched activators of the *CPSIT*_0429, D614G, and R346T targets was evaluated with the double mismatch versus single mismatch strategy.

specific, but only mut14/mut34 uniformly and significantly increased the signal-to-noise ratio of all three targets (Fig. 2c).

## Iterative design of crRNA dramatically increases specificity and maintains sensitivity

The introduction of single mismatched bases in the crRNA spacer is a common strategy for increasing the specificity of the CRISPR system. However, to achieve an optimal SNV detection signal-to-noise ratio, two criteria need to be satisfied after introducing a single mismatched base in the spacer: first, the detection signal for the unmutated target should be similar to the signal detected by WT crRNA; second, the detection signal of the mutated target should sharply decrease after the formation of a double base mismatch, similar to the signal detected by the NTC.

Coincidentally, the non-template strand (NTS) of each of the three targets we selected has a T-C mutation at position 14, forming an rU-dG base pairing in the spacer-TS DNA heteroduplex. When the spacer length was 17 bp, a T14C mutation in the NTS of the target did not result in a significant difference in analytical sensitivity compared to that of the wild type (Supplementary Fig. 6a, c, e), indicating that the free energy change (ΔG) of R-loop formation was almost unaffected. In a previous study exploring the effect of base mismatches on the binding energy of Cas12a, the single-base mutation of NTS T14C caused the smallest increase in the dissociation rate of the mismatch position[40]. In addition, the rU-dG mismatch is the most common mismatch type resulting in off-target effects of the CRISPR system in vivo[41]. We speculate that these results occur because the rU-dG mismatch is a wobble base pair that has similar thermodynamic stability to Watson–Crick base pairs[14,42,43].

However, previous studies have reported that mismatches of different base pairs at most positions produce no significant difference in specificity[14,35]. This finding indicates that the difference in specificity of this type of mutation at position 14 may be dependent on spacer length. We mutated the DNA at position 14 of the NTS of the target to three other bases and found significant differences at 17 bp, while the differences were not significant at 20, 19, or 18 bp, suggesting that this difference in the energetics of base complementary pairing manifests only at the point when the R-loop energy collapses (Fig. 3a), verifying that the R-loop energy at 20 bp is excessive[25,44].

Therefore, we mutated position 14 of the spacer-TS DNA heteroduplex at a length of 17 bp to form 16 DNA–RNA pairing combinations. Only rU-dG, rG-dT, and rC-dT base pairing showed minimal differences from the Watson–Crick base pairing (Fig. 3b). Both the rU-dG and rG-dT pairs are wobble base pairs, which are also a common mode of off-target mismatch in vivo, consistent with our previous speculation. In addition, rC-dT may accommodate base mismatches through double-stranded backbone rearrangement[41]. Moreover, there are many other T-C mutation positions in the NTC of the three targets, and with a 17 bp spacer, the wobble base pairing at most positions will still affect the ΔG of the R-loop, resulting in a significant decrease in the detection signal. Therefore, we speculate that the effect of wobble base pairing on the ΔG of the R-loop is position dependent.

We selected three templates with 17 bp spacer crRNAs for analytical sensitivity experiments for the NTC T-C mutation at positions 11, 9, and 12 of the *CPSIT*_0429, D614G, and R346T targets, respectively. Except for the T9C single mutation at the D614G target site, whose detection signal was not significantly different from that of the wild type, the analytical sensitivity at the other two positions was significantly decreased (Supplementary Fig. 6b, d, f). We also constructed templates for the NTC G-A mutation at position 14 and at other positions, and the sensitivity of the analysis of the three targets spacer-TS DNA heteroduplexes that form rG-dT wobble base pairs at position 14 did not significantly decrease. In contrast, there was a significant decrease at the other positions (Supplementary Fig. 7). The above results show that wobble base pairing at position 14 of the spacer-TS DNA heteroduplexes has little effect on the ΔG of the R-loop and suggest that the backbone sterics of the R-loop also affect the formation of the

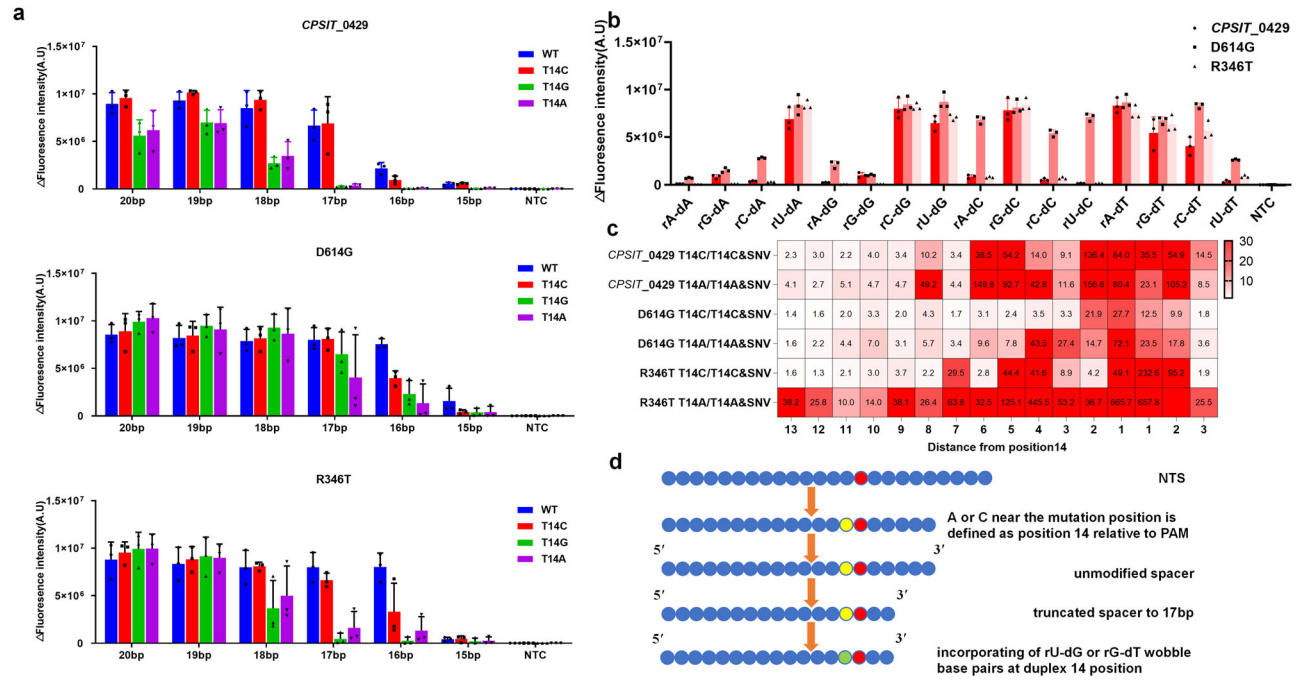


**Fig. 3 | Achieving high specificity by iterative crRNA design. a** Trans-cleavage activity of four DNA base types at position 14 of the non-template strand of three targets was tested against that of various crRNAs with different spacer lengths. **b** Trans-cleavage activity of four DNA base types and four RNA base types paired at R-loop position 14 for three targets. **c** The mismatch tolerance of crRNA with a 17 bp spacer was evaluated for different distances from the position 14 mismatched activator; in the case of the three targets, NTS was mutated to C or A, forming a rU-dG or rG-dT wobble pairing at position 14 in the spacer-TS DNA heteroduplex. Heatmap indicating the mean fold change in fluorescence value within 1 h for the activators containing the rU-dG or rG-dT wobble pair at position 14 in the 17 bp spacer-TS DNA heteroduplex, normalized to that of the corresponding distance mismatch activators. The values in the heatmap represent the multiples of specificity. **d** Schematic workflow of the iterative design of the crRNA spacer sequence based on the NTS sequence of the SNV target.

wobble base pair[41]. The strong signal of the T9C single mutation for the D614G target indicates that in addition to position 14 of the spacer-TS DNA heteroduplexes, there may be some rU-dG wobble base pairs at specific positions in the target that have little effect on the change in ΔG of the R-loop.

When the crRNA spacer was truncated to 17 bp, the introduction of spacer mismatches with TS DNA at position 14 followed the double mismatch versus single mismatch strategy, resulting in a significant decrease in the tolerance for single-base mismatches at the three target sites. The specificity enhancement is position dependent; in particular, the signal-to-noise ratio is almost 20 times greater at near position 14 (Supplementary Figs. 8–9 and Fig. 3c). Compared to that obtained when the crRNA spacer was truncated to 17 bp, the detection signal for single-base mutations at the three target sites was further reduced, leading to a further increase in specificity at each position on the target. This effect has a clear distance dependence, with the highest specificity increase occurring within 2 bases of position 14 (Supplementary Fig. 10). Moreover, in a previous study, in vitro cleavage experiments and in vivo phage competition experiments showed that two adjacent mismatches are more harmful than two distant mismatches[15]. Together, our results show that the specificity of Cas12a is dependent on the number, type, location, and distance of mismatches within the spacer-TS DNA heteroduplex.

Therefore, we designed an iterative crRNA design principle for detecting SNV sites (Fig. 3d): an A or C base was found at the nearest distance from the mutation position of the target NTC, preferably within 2 bases, defined as position 14 relative to the PAM. The length of the crRNA spacer was shortened to 17 bp, and position 14 of the spacer was changed to U or G to incorporate wobble base pairing at position 14 of the spacer-TS DNA heteroduplex.

## Underlying mechanisms of iterative design of crRNA for high specificity

Based on the aforementioned experimental findings, we propose an energy kinetic mechanism model that explains the achievement of high specificity and universality while maintaining sensitivity by iteratively modifying the crRNA through truncating the spacer to 17 bp and introducing wobble base pairing at position 14 of the spacer-TS DNA heteroduplex.

The specificity of the CRISPR system can be described by a simple two-step kinetic model of enzyme activity (Supplementary Fig. 11a). The two steps are binding (E + S = E•S) and cleavage (E•S = E + P) for both an on-target substrate and a mismatched off-target substrate. According to the current mainstream CRISPR model theory and in vitro/in vivo data, there is no significant difference in the $k_{on}$ between single-base mismatches and matched targets; thus, the specificity of CRISPR relies primarily on $k_{off}$ and $k_{cat}$[38,40,44–46].

Under normal conditions with a 20 bp spacer, the energy of base pair interactions that serve as the basis for target recognition is much greater than the energy required for cleavage, resulting in a higher energy barrier for dissociation of S from the E•S complex than for cleavage by the E•S complex, i.e., $k_{off} < k_{cat}$. Therefore, most E•S complexes undergo cleavage after binding. In the process of reversible R-loop expansion and collapse, mismatches can be considered energy penalties. The main reason for the inability of the CRISPR system to distinguish effectively between WT and SNV targets is that the energy barrier of the single-base mismatch penalty is insufficient to significantly increase $k_{off}$ above $k_{cat}$. Therefore, although unmodified crRNA maintains the sensitivity of the CRISPR system, single-base mismatches cannot be distinguished for almost all targets. Both an on-target substrate and a mismatched off-target substrate exhibit good amplification curves (Fig. 4a).

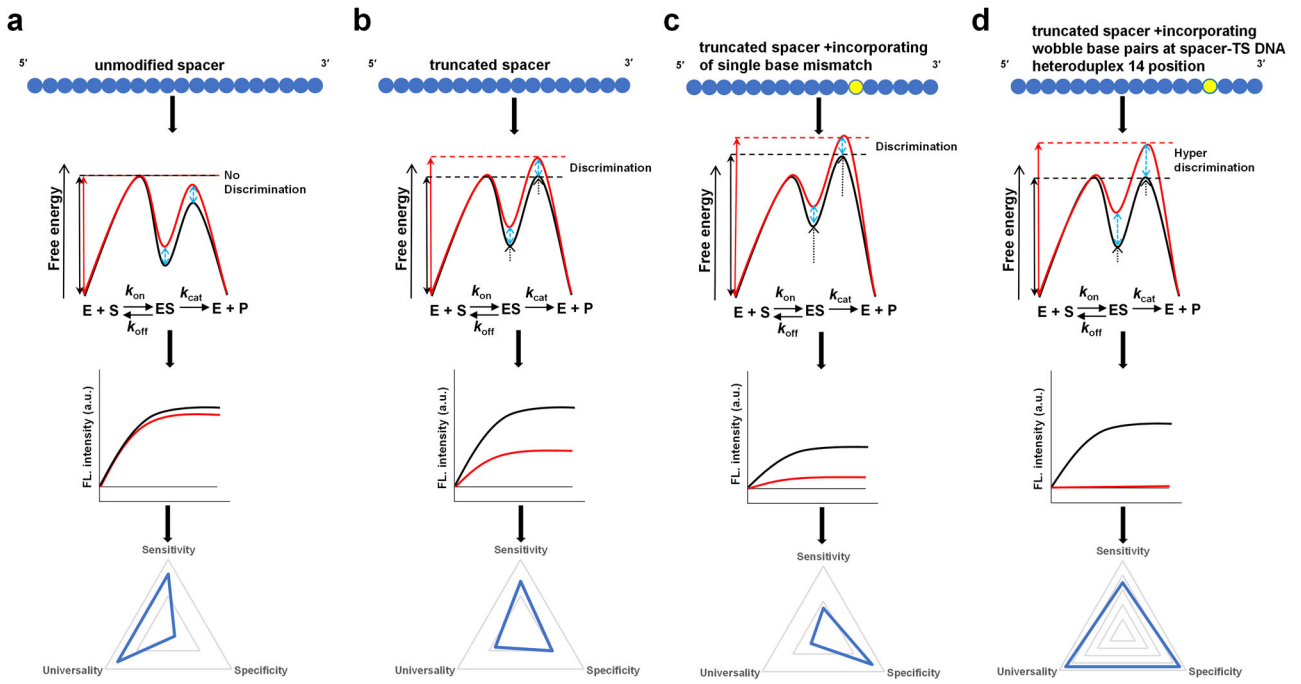


**Fig. 4 | Energy kinetic mechanism model of various crRNAs.** The model is divided into four parts from top to bottom. The first part represents the crRNA spacer region, where blue circles indicate matching bases and yellow circles indicate mismatched bases. The second part presents the two-step kinetic model of Cas12a/crRNA binding to the target substrate (black) and a mismatched off-target substrate (red) by using a free energy reaction diagram, where the wells represent states and the peaks represent the barriers for transitions between those states. The third part shows the amplification curves for the on-target and mismatched off-target substrates. The fourth part illustrates the sensitivity, specificity, and universality of Cas12a for various crRNAs using a triangular radar chart. **a** WT crRNA programmed with the Cas12a enzyme is unable to discriminate between on-target and a mismatched off-target substrate. **b** Truncated crRNA programmed with the Cas12a enzyme achieves specificity gains by increasing $k_{off}$ for both the on-target and a mismatched off-target substrate. **c** Truncated crRNA + single-base mismatch increases the specificity of Cas12a by greatly increasing $k_{off}$ for both the on-target and a mismatched off-target substrate. This promotes the dissociation of a mismatched off-target substrate but also reduces the cleavage of the on-target substrate, resulting in a decrease in sensitivity. **d** A truncated spacer + wobble base pairs at the spacer-TS DNA heteroduplex 14 position increases the specificity of Cas12a without sacrificing sensitivity by increasing $k_{off}$ and the mismatch penalty.

Currently, strategies to improve the specificity of CRISPR systems focus almost exclusively on increasing $k_{off}$ or decreasing $k_{cat}$ (Supplementary Fig. 11b and Supplementary Data 4). This makes the dissociation rate of the E•S complex higher than the rate of cleavage, causing most E•S complexes to undergo binding and dissociation equilibrium before cleavage occurs. Truncating the spacer length and reducing the number of base pairs formed with the target sequence weakens the energy of the target–guide interaction and intensifies R-loop instability, which is the most direct strategy for increasing $k_{off}$.

In this strategy, it is necessary to find the dynamic 'sweet spot' of the target, which is the point at which the energy of base pair interactions that form the basis for target recognition is approximately equal to the energy required for cleavage, i.e., $k_{off} \approx k_{cat}$. In this way, the cleavage activity of the Cas enzyme can be maintained as much as possible, and the penalty energy for single-base mismatches can increase the dissociation rate of mismatched targets, decreasing the cleavage of mismatched targets compared to that of matched targets and introducing a certain discriminatory ability. The amplification curves of an on-target substrate and a mismatched off-target substrate are different. In this study, 17 bp was the shortest length that increased $k_{off}$ for most targets and reduced the binding energy to the equilibrium point. Moreover, due to the small change in free energy caused by the single-base mismatch penalty and the different energetics of single-base mismatches at different positions and sequences, the differences in amplification curves at different sites of different targets may be large: thus the degree of specificity improvement is only moderate, and the universality is poor (Fig. 4b).

When the spacer is truncated, introducing an additional mismatched base significantly increases $k_{off}$ but also further increases the energy barrier for cleavage activity. In this case, the energy of the base pair interactions that serve as the basis for target recognition is lower than the energy required for cleavage, i.e., $k_{off} < k_{cat}$. On this basis, the penalty energy for single-base mismatches can further increase the dissociation rate of mismatched targets, decreasing the cleavage of mismatched targets compared to that of matched targets and thus introducing a certain discriminatory ability. Differences are thus observed in the amplification curves of on-target and off-target substrates. However, at the same time, the increase in $k_{off}$ decreases the amplification curves of both an on-target substrate and a mismatched off-target substrate. Notably, this strategy does not significantly improve the discrimination between mismatched and matched targets but rather affects the sensitivity to matched targets. Similarly, due to the different energy effects of single-base mismatches at different positions and sequences, the differences in amplification curves at different sites in different targets may be large (Fig. 4c).

Our research revealed that truncating the spacer to 17 bp and introducing a wobble base pair at position 14 of the spacer-TS DNA heteroduplex did not affect the free energy change of the R-loop. Based on this, we propose a new specificity enhancement strategy that increases the penalty energy for single-base mismatches to the level of double-base mismatches while also increasing $k_{off}$ (Supplementary Fig. 11b). In this strategy, the spacer is first truncated to 17 bp, making $k_{off} \approx k_{cat}$, and then wobble base pairing is introduced at position 14 without affecting ΔG and thus without further increasing the energy barrier to cleavage activity. As a result, this approach has a minimal impact on the amplification curve of an on-target substrate, ensuring high sensitivity. However, a mismatched off-target substrate results in a double base pair mismatch that strongly affects the formation of the R-loop, leading to a significant decrease in the amplification curve signal of mismatched targets, thereby ensuring high specificity (Fig. 4d). In summary, our strategy relies on the kinetics of the DNA target specificity of CRISPR/Cas12a, and it achieves universality and high specificity without sacrificing sensitivity.

## Development of a PAM-free one-pot platform

The PAM dependency of Cas12a for the recognition of double-stranded target sequences and the limited distance of the PAM from the wobble base pairing distance in the iterative crRNA design method constrains the detectable sequence range. Therefore, overcoming the limitations of PAM is extremely important for the application and promotion of this technology. Introducing PAM into the preamplification product provides an opportunity to remove sequence restrictions. Recently, several studies have introduced PAM sequences into PCR, LAMP, or RPA primers to overcome the limitations of PAM sequences[39,47,48].

In this study, we introduced the PAM sequence (TTTV) of Cas12a into the upstream primers of RPA and thus into the amplified products of three selected target sites. Specifically, we inserted 0–3 bp at every other base pair from the 3′ end to the 5′ end of the upstream primers used for RPA, thereby introducing the PAM sequence between the first and second bases, between the second and third bases, and so on, to construct upstream primers with PAM sites at different positions. Subsequently, the upstream primers were separately subjected to RPA amplification reactions with the downstream primers, thereby locating the first base after the upstream primer sequence at distances of −1 to 14 bases from the PAM site to obtain amplified products containing PAM sites at different positions (Fig. 5a).

To verify whether the PAM sequence was correctly inserted, we sequenced the amplified product and found that the insertion of the PAM sequence near the 3′ end of the primer affected the accuracy of the adjacent sequence (Fig. 5b and Supplementary Figs. 12–14). Products with distances of −1 and 1–3 from the PAM site could not be amplified correctly, while products with other distances from the PAM site could be introduced correctly without any mutations or deletions in the adjacent bases. This finding indicated that the 3′ end of the RPA primer was intolerant to insertion, which was consistent with the conclusions of other published studies[49]. As observed in Fig. 5b, all three targeted sequences were accurately amplified when the insertion was at position 0. The reason behind this phenomenon can be attributed to the specific nature of the expected sequences for these targets. For both *CPSIT*_0429 and R346T, the expected sequence aligns perfectly with their original sequences when the PAM sequence is inserted at position 0. Similarly, the D614G target has only a minimal difference of one thymine base from its native sequence under this condition.

To determine whether the insertion of the PAM sequence affected the analytical sensitivity of the RPA-CRISPR reaction, we selected the upstream primer sequences of the three target sites highlighted in yellow in Fig. 5b for RPA reactions. PAM sequence insertions at different distances were constructed, with position 9 for the *CPSIT*_0429 target, position 3 for the D614G target, and position 4 for the R346T target relative to the PAM site. The subsequent two-step analytical sensitivity experiment revealed that the sensitivity to the *CPSIT*_0429 target and the R346T target was not affected, while the detection limit of the D614G target was significantly reduced, indicating that correctly inserted PAM sequences did not affect the analytical sensitivity of the RPA-CRISPR reaction, while incorrectly inserted PAM sequences decreased the sensitivity (Fig. 5c). The above results indicated that we can establish a method to introduce the PAM sequence by inserting bases at positions 4-15 from the 3′ end of the upstream primer in RPA, thereby overcoming the PAM limitation of CRISPR detection and eliminating the position requirement during iterative crRNA design.

The one-pot reaction of RPA and CRISPR not only decreases total detection time and reduces the number of operational steps but also presents the additional advantage of eliminating aerosol contamination, which is also crucial for the promotion and application of this technology. A recent report revealed that glycerol additives can slow the fusion of RPA and CRISPR systems, thereby enabling one-pot detection[50]. We tested this method by first screening various volume ratios and concentrations for glycerol addition and found that a 20% concentration yielded the best signal for one-pot detection (Supplementary Fig. 15). Therefore, we used 20% glycerol for further experiments. Sensitivity analysis revealed that the addition of 20% glycerol decreased the detection limit of three analytes in a one-pot RPA assay compared to that of glycerol-free one-pot detection, thus making one-pot detection feasible (Supplementary Fig. 16). As a result, we established a one-pot RPA-CRISPR detection method without PAM restriction.

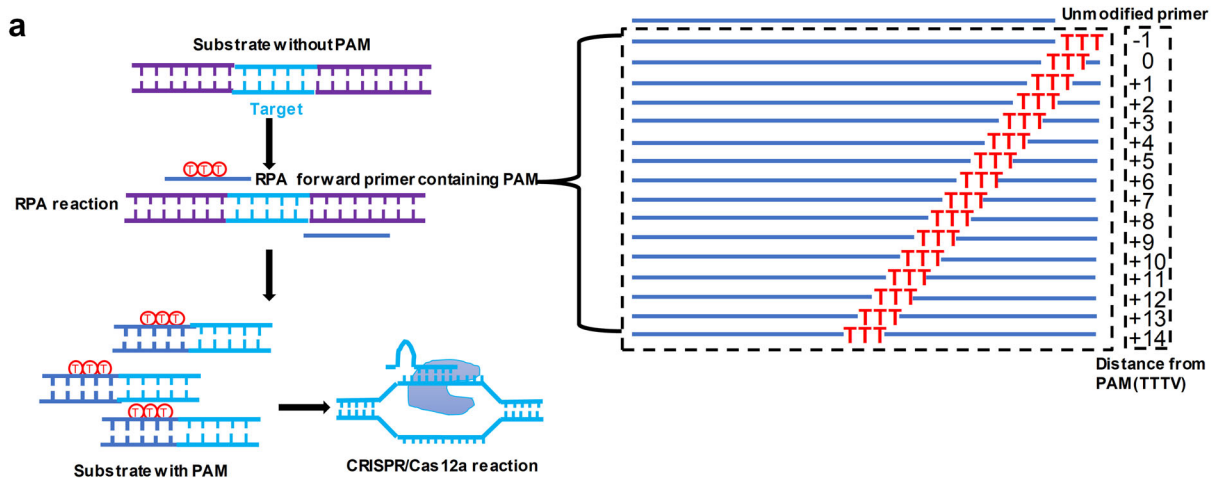


**b**

| *CPSIT*_0429 | | Match | D614G | | Match | R346T | | Match | |
|---|---|---|---|---|---|---|---|---|---|
| Expected sequence | Sanger sequencing data | (Y/N) | Expected sequence | Sanger sequencing data | (Y/N) | Expected sequence | Sanger sequencing data | (Y/N) | |
| agcgtgtaaggttta**gattct** | agcgtgtaaggttta**gattct** | Y | cttctaaccaggttg**ctgttc** | cttctaaccaggttg**ctgttc** | Y | ctattgttagatttc**ctaata** | ctattgttagatttc**ctaata** | Y | U |
| agcgtgtaaggttta**TTTgattct** | agcgtgtaaggttta**TTTtcttta** | N | cttctaaccaggttg**TTTctgttc** | cttctaaccaggttg**TTTtcttta** | N | ctattgttagatttc**TTTctaata** | ctattgttagatttc**TTTctgtag** | N | -1 |
| agcgtgtaagg**TTTa**gattct | agcgtgtaagg**TTTa**gattct | Y | cttctaaccagg**TTTg**ctgttc | cttctaaccagg**TTTg**ctgttc | Y | ctattgttaga**TTTc**ctaata | ctattgttaga**TTTc**ctaata | Y | 0 |
| agcgtgtaagg**TTTca**gattct | agcgtgtaagg**TTTca**ttctt | N | cttctaaccagg**TTTcg**ctgttc | cttctaaccagg**TTTcg**ttctta | N | ctattgttaga**TTTcc**taata | ctattgttaga**TTTcc**taatat | N | 1 |
| agcgtgtaagg**TTTcta**gattct | agcgtgtaagg**TTTcta**ttctt | N | cttctaaccagg**TTTctg**ctgttc | cttctaaccagg**TTTctg**ttctt | N | ctattgttaga**TTTctc**taata | ctattgttaga**TTTctc**tgtaga | N | 2 |
| agcgtgtaagg**TTTctta**gattct | agcgtgtaagg**TTTctta**gattct | Y | cttctaaccag**TTTgttg**ctgttc | cttctaaccag**TTTgttg**ttcttt | N | ctattgttaga**TTTcttc**taata | ctattgttaga**TTTcttc**tgtaga | N | 3 |
| agcgtgtaag**TTTgttta**gattct | agcgtgtaag**TTTgttta**gattct | Y | cttctaacca**TTTggttg**ctgttc | cttctaacca**TTTggttg**ctgttc | Y | ctattgttag**TTTatttc**taata | ctattgttag**TTTatttc**taata | Y | 4 |
| agcgtgtaa**TTTggttta**gattct | agcgtgtaa**TTTggttta**gattct | Y | cttctaacc**TTTaggttg**ctgttc | cttctaacc**TTTaggttg**ctgttc | Y | ctattgtta**TTTgatttc**taata | ctattgtta**TTTgatttc**taata | Y | 5 |
| agcgtgta**TTTaggttta**gattct | agcgtgta**TTTaggttta**gattct | Y | cttctaac**TTTcaggttg**ctgttc | cttctaac**TTTcaggttg**ctgttc | Y | ctattg**TTTagatttc**taata | ctattg**TTTagatttc**taata | Y | 6 |
| agcgtg**TTTaaggttta**gattct | agcgtg**TTTaaggttta**gattct | Y | cttctaa**TTTccaggttg**ctgttc | cttctaa**TTTccaggttg**ctgttc | Y | ctattg**TTTcagatttc**taata | ctattg**TTTcagatttc**taata | Y | 7 |
| agcgtg**TTTcaaggttta**gattct | agcgtg**TTTcaaggttta**gattct | Y | cttcta**TTTaccaggttg**ctgttc | cttcta**TTTaccaggttg**ctgttc | Y | ctattg**TTTctagatttc**taata | ctattg**TTTctagatttc**taata | Y | 8 |
| agcg**TTTgtaaggttta**gattct | agcg**TTTgtaaggttta**gattct | Y | cttc**TTTaaccaggttg**ctgttc | cttc**TTTaaccaggttg**ctgttc | Y | cta**TTTgttagatttc**taata | cta**TTTgttagatttc**taata | Y | 9 |
| agcg**TTTcgtaaggttta**gattct | agcg**TTTcgtaaggttta**gattct | Y | cttc**TTTcaaccaggttg**ctgttc | cttc**TTTcaaccaggttg**ctgttc | Y | cta**TTTcgttagatttc**taata | cta**TTTcgttagatttc**taata | Y | 10 |
| agc**TTTgtgtaaggttta**gattct | agc**TTTgtgtaaggttta**gattct | Y | c**TTTctaaccaggttg**ctgttc | c**TTTctaaccaggttg**ctgttc | Y | cta**TTTctgttagatttc**taata | cta**TTTctgttagatttc**taata | Y | 11 |
| ag**TTTcgtgtaaggttta**gattct | ag**TTTcgtgtaaggttta**gattct | Y | c**TTTcctaaccaggttg**ctgttc | c**TTTcctaaccaggttg**ctgttc | Y | c**TTTattgttagatttc**taata | c**TTTattgttagatttc**taata | Y | 12 |
| a**TTTgcgtgtaaggttta**gattct | a**TTTgcgtgtaaggttta**gattct | Y | c**TTTctctaaccaggttg**ctgttc | c**TTTctctaaccaggttg**ctgttc | Y | c**TTTcattgttagatttc**taata | c**TTTcattgttagatttc**taata | Y | 13 |
| **TTTagcgtgtaaggttta**gattct | **TTTagcgtgtaaggttta**gattct | Y | **TTTcttctaaccaggttg**ctgttc | **TTTcttctaaccaggttg**ctgttc | Y | **TTTctattgttagatttc**taata | **TTTctattgttagatttc**taata | Y | 14 |

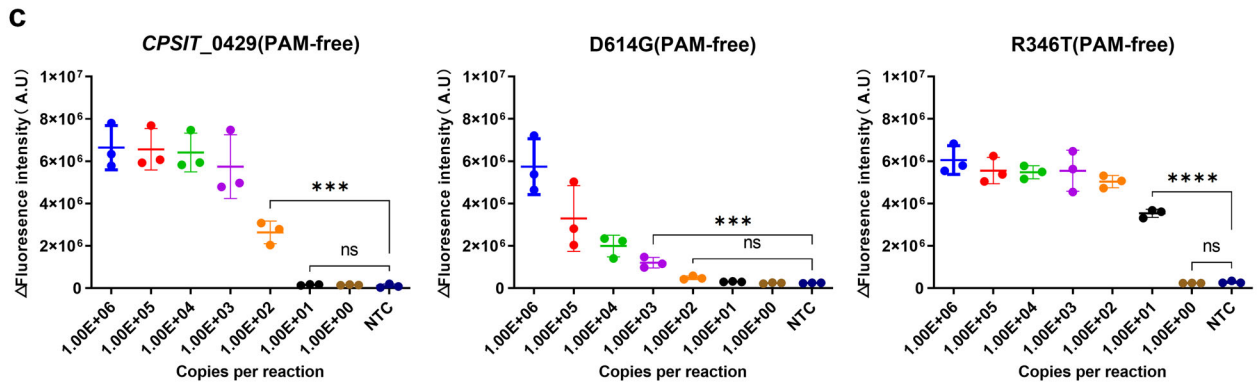


**Fig. 5 | Development of a PAM-free platform. a** Schematic diagram of the PAM sequence introduced at different positions on the RPA forward primers. **b** Comparison between the expected sequence and the Sanger sequencing data of the amplification products of three targets. The green sequence represents the amplified product sequence after the PRA forward primer. The lower case red sequence represents the Sanger sequencing data, which does not match the expected sequence. The right side of the figure represents the distance between the amplification product after the PRA primer and PAM (TTTV), while 'U' represents the unmodified sequence. Y, yes; N, no. The sequences marked in yellow represent the corresponding PAM-containing RPA forward primer that we selected for sensitivity analysis in the subsequent analysis. All the RPA primer sequences are provided in Supplementary Data 5. **c** Analytical sensitivity of two-step reactions of the three targets using a PAM-containing RPA forward primer and a PAM-free target activator. The target substrate was tenfold serially diluted to concentrations ranging from $10^6$ to $10^0$ copies per reaction. Error bars represent mean ± SD, $n = 3$. $^{***}P < 0.001$, $^{****}P < 0.0001$; ns not significant.

## Application of the designed platform to detect SARS-CoV-2 variants

In light of the recent COVID-19 pandemic, the rapid and accurate detection of SARS-CoV-2 variants will greatly promote efficient monitoring and precise tracing of viral mutations[51]. Based on the list of variations in lineages downloaded from the SARS-CoV-2 Variations Evaluation and Prewarning System at https://nmdc.cn/ncovn/lineage (Supplementary Data 6), we targeted two common variant strains, BA.5.2 and XBB, and performed iterative design of crRNAs to detect two unique mutations, T1050N (a unique mutation of BA.5.2) and Q183E (a unique mutation of XBB), based on their non-template strand sequences at point mutation sites (Supplementary Fig. 17).

The SNV crRNA we designed for these targets can effectively distinguish whether single nucleotide mutations have occurred in simulated samples (Q183E and T1050N targets synthesized in vitro) ($p < 0.0001$) (Supplementary Fig. 18a). In the presence of the unmutated template, the signal intensity of the SNV crRNA decreased sharply, with no significant difference compared to the NTC detection signal. In the presence of the

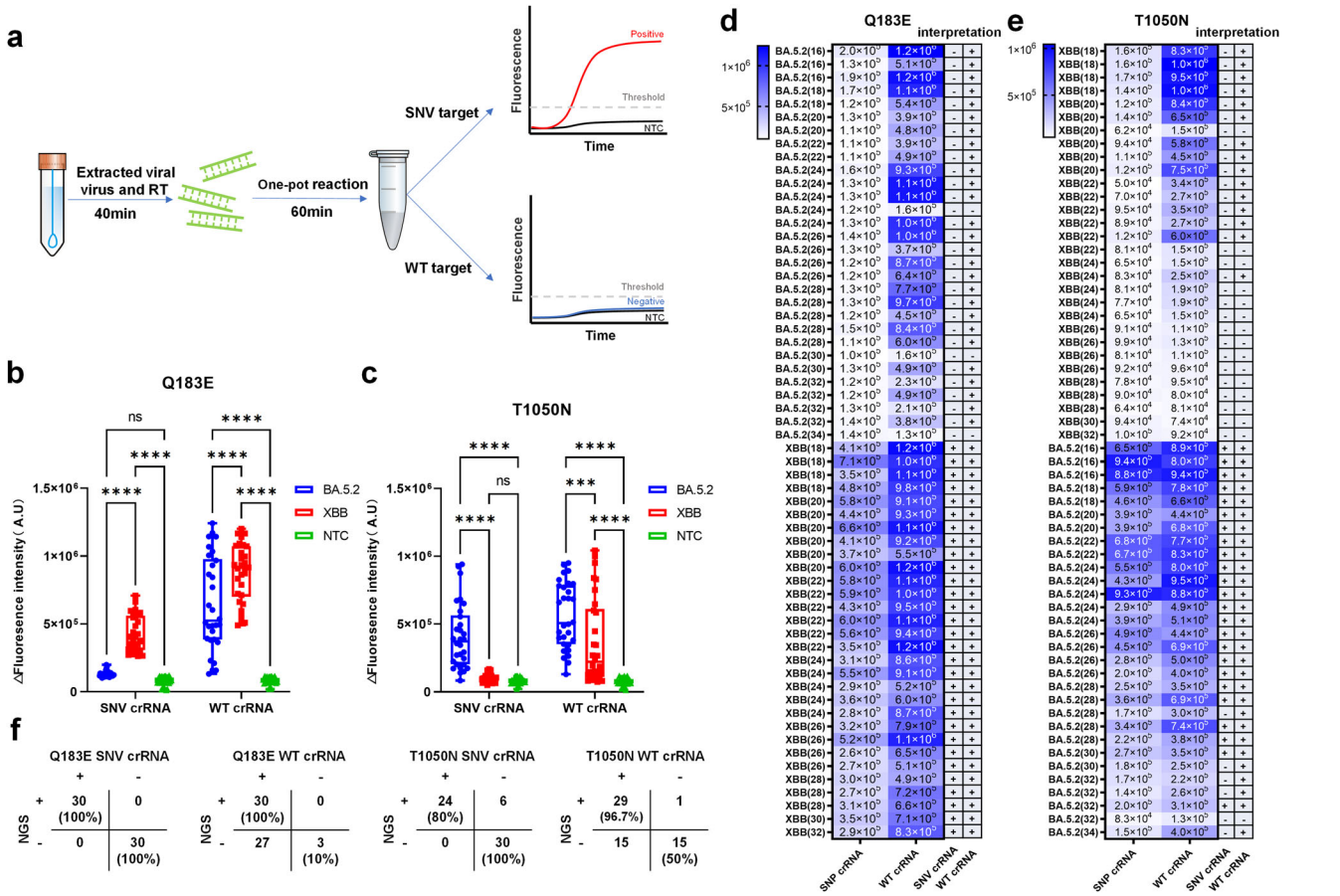


**Fig. 6 | Detection of Q183E and T1050N SNVs in SARS-CoV-2. a** Schematic workflow of the SARS-CoV-2 variant detection platform. **b**, **c** Box and whiskers plots of 60 clinical SARS-CoV-2 samples (30 BA.5.2 strains and 30 XBB-positive strains verified by NGS) were evaluated using the corresponding SNV crRNA and WT crRNA. NTC, non-target control. $n = 3$. $^{***}P < 0.001$, $^{****}P < 0.0001$; ns not significant. **d**, **e** Heatmap indicating the trans-cleavage activity of the Q183E or T1050N targets tested against the corresponding SNP crRNA or WT crRNA. The values in the heatmap represent the mean fluorescence value increase within 1 h. When this value is greater than $2 \times 10^5$, the sample is interpreted as positive (+), and when this value is less than or equal to $2 \times 10^5$, the sample is interpreted as negative (−). The left side shows the SARS-CoV-2 variant and its CT value. The right side shows the positive (+) or negative (−) result. **f** The results of the NGS and CRISPR/Cas12a were consistent with those of the corresponding SNV crRNA and WT crRNA for the detection of the SARS-CoV-2 variants XBB ($n = 30$) and BA.5.2 ($n = 30$). True-positive and true-negative percentage agreements are shown in parentheses.

mutated template, SNV crRNA had a clear detection signal, and its analytical sensitivity was consistent with that of WT crRNA for the detection of unmutated templates, at $10^2$ copies per reaction (Supplementary Fig. 18b,c). To further validate our crRNA design strategy for different GC contents, we also tested it on low GC targets (gyrA E88K and gyrA S112 = ) and high GC targets (rpoB H445D and rpoB S450L). As shown in Supplementary Fig. 19, our method can effectively distinguish between wild-type and mutant targets across a range of GC contents, supporting the broad applicability of our strategy.

Moreover, we collected 60 confirmed COVID-19-positive clinical throat swab samples (including 30 strains verified by high-throughput sequencing BA5.2 and XBB) and 30 negative clinical samples. We established a PAM-free and highly sensitive one-pot detection platform with high mutation resolution (Fig. 6a). To ensure the reliability of the detection, each sample was tested three times. We designed an SNV crRNA targeting the single-base mutation site Q183E, which can significantly distinguish between BA.5.2 and XBB mutant strains ($p < 0.0001$). In the presence of the XBB mutant strain, the Q183E SNV crRNA clearly detected the signal, while in the presence of the BA.5.2 mutant strain, the detection signal of the Q183E SNV crRNA sharply decreased, with no significant difference compared to the NTC detection signal. However, the Q183E WT crRNA did not distinguish between the BA.5.2 and XBB mutant strains, as the difference was not significant. Conversely, the SNV crRNA designed to target the single-base mutation site T050N significantly distinguished between the BA.5.2 and XBB mutant strains ($p < 0.0001$). In the presence of the BA.5.2 mutant strain, T1050N SNV crRNA exhibited a clear detection signal, while in the presence of the XBB mutant strain, the detection signal of T1050N SNV crRNA sharply decreased, with no significant difference compared to the NTC detection signal. Similarly, T1050N WT crRNA did not distinguish between the BA.5.2 and XBB mutant strains, as the difference was not significant (Fig. 6b, c).

By performing receiver operating characteristic (ROC) curve analysis on the fluorescence results of the SARS-CoV-2 samples after 1 h using Q183E SNV crRNA and T1050N SNV crRNA (Supplementary Fig. 20), we observed area under the curve (AUC) values of 1.0 and 0.97, respectively, indicating a high discriminative ability between the positive and negative samples. In contrast, the AUC values for the Q183E WT crRNA and T1050N WT crRNA were 0.71 and 0.72, respectively, suggesting that the iteratively designed SNV crRNA outperformed the WT crRNA in distinguishing single-nucleotide mutations. Based on the fluorescence values obtained by 30 NTC samples for both the Q183E and T1050N targets, we set the fluorescence threshold at three times the mean fluorescence increase, which was approximately $2 \times 10^5$ (Supplementary Fig. 21). Given this threshold, we determined the positivity or negativity of the detection results, which showed good consistency with the sequencing results, confirming the accuracy and reliability of our platform (Fig. 6d, e). Notably,

most of the samples with undetected T1050N SNV crRNA had Ct values less than 30.

The positive percentage agreement (PPA) for detecting XBB mutant strains using Q183E SNV crRNA was 100%, while the negative percentage agreement (NPA) was also 100%. However, when using the Q183E WT crRNA, the PPA remained 100%, but the NPA decreased sharply to only 10%. For detecting BA.5.2 mutant strains using T1050N SNV crRNA, the PPA was 80%, the NPA was 100%, the PPA for WT crRNA was 96.7%, and the NPA was only 50% (Fig. 6f). The concordance table between the CRISPR and NGS results showed that, compared with the WT crRNA, the SNV crRNA greatly improved the NPA and the discrimination of single nucleotide mutations. Taken together, these results demonstrate that our detection method can efficiently, accurately, and rapidly detect SNVs.

## Discussion

CRISPR detection is an emerging nucleic acid detection technology. Although the powerful signal amplification capability of the CRISPR system can be combined with amplification techniques to maintain its high sensitivity for target DNA recognition, the application of CRISPR detection methods for SNV detection has been limited. Cas proteins, such as Cas12a and Cas9, are described by a common "excess energy" theoretical model structure used in specificity research: when the binding energy exceeds a certain threshold, they can stably bind to both correct and incorrect targets. Single-bp mismatches in R-loops can provide only limited barriers, and the fidelity of the system is thus controlled kinetically. This model is also the theoretical basis for the off-target effects of Cas enzymes and the inability to achieve single-base resolution[44]. Moreover, target specificity depends on the number, type, and position of mismatches within the guide-target heteroduplex, making it particularly difficult to create a universal, highly specific, and sensitive detection method.

In this study, we identified four ways to significantly improve the cis-cleavage specificity of the Cas12a enzyme by modifying different regions of the crRNA secondary structure. Among them, M39 (scaffold engineering: 3′ truncation 1 bp) and M42 + M43 (loop engineering: 3′ split), might reduce the affinity between crRNA and Cas12a, affecting the stability of R-loop formation and increasing the specificity. M63 (extension engineering: 3′ foldback blocking 15 bp), might increase specificity by forming a hairpin secondary structure on the spacer, thereby affecting R-loop formation. The specificity-enhancing effects of both M42 + M43 and M63 in CRISPR gene editing have been successfully validated[22,52]. However, the degree of specificity enhancement of these three methods is insufficient, and some sensitivity is lost.

A truncated spacer is a preferable option. Fu et al. previously reported that using a sgRNA with a spacer length of 17–18 bp could significantly reduce the off-target effects of the sgRNA without sacrificing sensitivity[25]. Zhang et al. reported that a 17 bp spacer can reduce off-target effects but may decrease gene editing efficiency in certain cell lines[53]. These two articles indicated that using a sgRNA with a 17 bp spacer can maximize Cas9 cleavage activity while increasing specificity. Similarly, FnCas12a can maintain the same gene editing efficiency as untruncated crRNA when the spacer is truncated to 16 bp-17 bp, and single-base mutations can be discriminated if the 3′ end of the corresponding target crRNA is truncated as much as possible[24]. This study provides a detailed investigation of the impact of truncating the crRNA spacer region on the trans-cleavage specificity of the CRISPR/Cas12a system in vitro. Although the specificity for single- and double-base mutations increases with increasing truncation of the spacer, the maximum truncation length varies for different targets. The 17 bp spacer was the shortest length that generally maintained Cas12a activity. However, relying solely on truncating the crRNA spacer to improve specificity is insufficient.

The crRNA-modified single-nucleotide mutation experiment indicated that mismatches in the PAM proximal and PAM distal regions had little effect on trans-cleavage activity, while previous literature suggested that mismatches in the PAM proximal region had a greater impact on cis-cleavage[12]. These results demonstrated the importance of perfect pairing in the PAM proximal region for the cis-cleavage activity of the Cas12 protein, but this pairing is not necessary for trans-cleavage activation[54]. The sequence in the middle region of the spacer is sensitive to mismatch because it directly interacts with the middle double-stranded region of the TS DNA and the Helical II of the Cas12 protein, affecting its conformation, which is essential for the activation of the RuvC catalytic pocket[55]. An experiment involving adjacent double nucleotide mutations showed that the energy penalty for double nucleotide mismatches is much greater than that for single nucleotide mismatches. However, the double mismatch versus single mismatch strategy alone is insufficient because the characteristics of adjacent mismatches strongly affect the formation of the R-loop. This strategy also requires consideration of how to avoid sensitivity to single nucleotide mismatches and the problems of target and sequence specificity.

This study revealed that when the spacer was truncated to 17 bp, position 14 of the R-loop was a special position: wobble base pairing at this position had almost no effect on the stability of the R-loop. The following reasons are proposed: 1. The thermodynamic stability of the fluctuating base pair is comparable to that of the Watson–Crick base pair, and rU-dG pairing is also a common in vivo off-target pairing that is conducive to the formation of heteroduplexes. 2. The steric hindrance of the backbone may also affect the formation of heteroduplexes, position 14 of the spacer-TS DNA heteroduplex may be subject to less steric restriction[41].

On the basis of this finding, we developed a new strategy to increase specificity through simple iterative modification of crRNA. By increasing $k_{off}$ and the single mismatch penalty, we achieved high specificity while maintaining sensitivity and universality. Our crRNA modification method requires only the identification of an A or C base within 2 bases of the mutation site, which is very easy in genomic sequences, thus ensuring its ease of use.

This study established a SARS-CoV-2 point mutation detection platform based on RPA-CRISPR/Cas12a technology. The assay platform has the following characteristics: one-pot operation, high specificity without sacrificing sensitivity, and high universality achieved by a simple and convenient crRNA modification method, which facilitates commercial promotion and the rapid adjustment of protocols in the face of emerging variants. However, further improvements in the detection system are needed to ensure that the system is suitable for low Ct value samples, and additional real samples need to be collected to verify the reliability and stability of this scheme.

Finally, we believe that our study provides new insights into the specificity of Cas enzymes. This approach provides not only a promising and market-competitive in vitro diagnostic tool for SNVs but also the possibility of improving the safety of gene therapy by preventing off-target effects of in vivo gene editing.

## Methods

### Materials

The LbCas12a and NEBuffer 2.1 were purchased from New England Biolabs (Beijing, China). All the crRNAs, RPA primers, templates, and ssDNA-FQ reporter (FAM-TTTTTTTTTTTT-BHQ1) were synthesized by GENEWIZ (Suzhou, China) and can be found in the Supplementary Data. SuperScript IV reverse transcriptase (200 U/μL), nuclease-free water, and glycerol were purchased from Thermo Fisher Scientific (Shanghai, China). A TwistAmp Basic Kit was purchased from TwistDX, Inc (England). A Novel Coronavirus (2019) Nucleic Acid Detection Kit was purchased from BioProfectus Co., Ltd (Taizhou, China). A Nucleic acid rapid extraction kit (magnetic bead method) was purchased from Zybio Inc. (Chongqing, China). A SynScript™ III cDNA Synthesis Mix was purchased from Tsingke Biotechnology Co., Ltd. (Beijing, China). Fragments of the SARS-CoV-2(GenBank accession: NC_045512.2) or *Chlamydia psittaci* (GenBank accession: CP002549.1) genome containing the D614G, R346T, Q183E, or T1050N mutation site or the *CPSIT*_0429 site were selected as targets.

### Sample preparation

Throat swab specimens were used as the source of viral RNA templates and were obtained from the National Novel Coronavirus Surveillance Network Laboratory of the Changzhou Center for Disease Control and Prevention. Viral RNA templates were extracted by an automatic nucleic acid extraction instrument and nucleic acid rapid extraction kit (magnetic bead method). The RT-qPCR assay was performed according to the instructions provided in the Novel Coronavirus (2019) Nucleic Acid Detection Kit. The reaction was performed as follows: 1 cycle of reverse transcription at 50 °C for 10 min, 1 cycle of predenaturation at 97 °C for 1 min, 40 cycles of denaturation at 97 °C for 5 s for annealing, and extension at 58 °C for 30 s. The fluorescence signal from the PCR was monitored at each extension step using an Applied Biosystems® QuantStudio Q5 (ABI Q5) instrument. The reverse transcription assay was performed according to the instructions provided with the SynScript™ III cDNA Synthesis Mix. A total reaction volume of 20 μL was used, consisting of 10 μL of extracted RNA, 4 μL of 5x RT Reaction Mix, 1 μL of SynScript™ III RT Enzyme Mix, and 5 μL of RNase-free water. The reaction was performed as follows: 25 °C for 10 min, 50 °C for 15 min, and 85 °C for 5 min. The reverse transcription products were placed in an ice box for use or stored at −80 °C.

### Recombinase Polymerase Amplification (RPA) assay

The primer sequences were designed based on the instructions of the TwistAmp™ Reaction Kit. The RPA reaction was performed according to the instructions of the TwistAmp® Basic Kit (TwistDx). The reaction mixture was as follows: 29.5 μL of primer-free rehydration buffer, 11.2 μL of nuclease-free water, and 2.4 μ of each of the forward and reverse primers (10 μM) were mixed in an Eppendorf tube and added to the reaction tube containing the lyophilized RPA enzyme. Two microlitres of template DNA and 2.5 μL of magnesium acetate (280 nM) were subsequently added, for a total volume of 50 μL. The mixture was vortexed until the lyophilized powder of the RPA enzyme was completely dissolved, followed by brief centrifugation. The reaction tube was then incubated at 37 °C in a metal thermocycler for 30 min. The sequencing of the RPA amplification products was completed by GENEWIZ, including the purification and recovery of the reaction products, followed by TA cloning and selection of 3–5 clones for Sanger sequencing.

### CRISPR/Cas12a detection assay

The Cas12a/crRNA nucleic acid detection system consisted of 1 μL of LbCas12a (5 μM), 1 μL of crRNA (5 μM), 2 μL of the ssDNA-FQ reporter (10 μM), and 5 μL of NEBuffer 2.1 (10×) in each reaction tube. Then, an appropriate volume of template DNA or RPA product was added, followed by nuclease-free water to reach a final volume of 50 μL. After shaking and centrifugation, the reaction tube was immediately incubated in an ABI Q5 instrument at 37 °C for 1 h, after which the fluorescence signal was recorded every minute. For the single (double) base-specific detection assay, in vitro synthesized dsDNA templates with single base mutations in the 20 bp region paired with the spacer (total of 20) and dsDNA templates with double base mutations in the 20 bp region paired with the spacer (total of 19) were used. Different crRNA mutants were subsequently added to the CRISPR/Cas12a reaction system. The specificity of the crRNA mutants was determined by observing the strength of the fluorescence signal compared to that of the unmodified crRNA.

### RPA coupled with CRISPR/Cas12a in a one-pot reaction

RPA-CRISPR/Cas12a one-pot reaction assays were performed as previously[50] described with some modifications. Briefly, for the one-pot reaction system, components A and B were prepared in advance. Component A consisted of the RPA system, which was prepared by mixing 29.5 μL of Primer Free Rehydration buffer, 11.2 μL of Nuclease-Free Water, and 2.4 μL of each of the upstream and downstream primers (10 μM) in an Eppendorf tube. The mixture was subsequently added to a reaction tube containing lyophilized RPA enzyme, followed by the addition of 2 μL of template DNA. The tube was vortexed and centrifuged. Component B consisted of 1 μL of LbCas12a (5 μM), 1 μL of crRNA (5 μM), 2 μL of the ssDNA-FQ reporter (5 μM), 5 μL of NEBuffer 2.1 (10×), 40% (v/v) glycerol, and nuclease-free water to a total volume of 50 μL. The mixture was vortexed and centrifuged, and 10 μL of component B was added to the bottom of the reaction tube, followed by the addition of 9 μL of component A and 1 μL of magnesium acetate (280 nM) to the side of the tube. The reaction tube was covered and placed in a centrifuge for slow and brief centrifugation and then incubated in an ABI Q5 instrument at 37 °C for 1 h. Fluorescence values were collected and recorded every minute.

### High-throughput sequencing

For the PCR-positive SARS-CoV-2 samples, RNA was extracted using random hexamers and annealed, followed by reverse transcription into first-strand cDNA. Two separate PCR amplifications were performed on the cDNA, after which the EBLST fragment was amplified, and the adapter sequence was added. The amplified product with the adapter was cleaned. The PCR program was used to amplify the fragmented and labeled products. The PCR procedure involved the addition of the prepaired 10 bp tag 1 (i7) adapter, tag 2 (i5) adapter, and sequence required for sequencing cluster generation. All the prepared libraries were mixed in one tube, cleaned and purified. A Qubit dsDNA HS Assay Kit was used to analyse 2 μL of the mixed library. If the library was out of the standard range, it was diluted 1:10 and analysed again. The library was then diluted to a uniform concentration of 4 nM using RSB or water according to the denaturation and dilution guidelines of the system used and loaded onto the iSeq 100 or MiSeq after insertion into the sequencing cartridge.

### Statistics and reproducibility

GraphPad Prism 9 was used for all the statistical analyses. Each experiment was repeated three times. The data are presented as the mean ± standard deviation (SD). One-way ANOVA was used for multigroup comparisons. Differences were considered statistically significant at $P < 0.05$.

### Reporting summary

Further information on research design is available in the Nature Portfolio Reporting Summary linked to this article.

## Data availability

Primer and crRNA sequences and other data supporting the findings of this study are available in the paper and its Supplementary Information files. The high-throughput sequencing data have been deposited with the Sequence Read Archive under the BioProject accession: PRJNA1057968. Source data are available in the Source Data file. Other datasets generated during the current study are available from the corresponding author on reasonable request.

Received: 19 March 2024; Accepted: 30 October 2024;
Published online: 07 November 2024

## References

1. Pickar-Oliver, A. & Gersbach, C. A. The next generation of CRISPR-Cas technologies and applications. *Nat. Rev. Mol. Cell Biol.* **20**, 490–507 (2019).
2. Yang, H. et al. CRISPR-based nucleic acid diagnostics for pathogens. *Trends Anal. Chem.* **160**, 116980 (2023).
3. Stella, S. et al. Conformational activation promotes CRISPR-Cas12a catalysis and resetting of the endonuclease activity. *Cell* **175**, 1856–1871.e1821 (2018).
4. Cofsky, J. C. et al. CRISPR-Cas12a exploits R-loop asymmetry to form double-strand breaks. *Elife* **9**, https://doi.org/10.7554/eLife.55143 (2020).
5. Naqvi, M. M., Lee, L., Montaguth, O. E. T., Diffin, F. M. & Szczelkun, M. D. CRISPR-Cas12a-mediated DNA clamping triggers target-strand cleavage. *Nat. Chem. Biol.* **18**, 1014–1022 (2022).

6. Swarts, D. C. & Jinek, M. Mechanistic Insights into the cis- and trans-Acting DNase Activities of Cas12a. *Mol. Cell* **73**, 589–600.e584 (2019).
7. Pacesa, M. et al. R-loop formation and conformational activation mechanisms of Cas9. *Nature* **609**, 191–196 (2022).
8. Swarts, D. C., van der Oost, J. & Jinek, M. Structural basis for guide RNA processing and seed-dependent DNA targeting by CRISPR-Cas12a. *Mol. Cell* **66**, 221–233.e224 (2017).
9. Chen, J. S. et al. CRISPR-Cas12a target binding unleashes indiscriminate single-stranded DNase activity. *Science* **360**, 436–439 (2018).
10. Li, Y., Li, S., Wang, J. & Liu, G. CRISPR/Cas systems towards next-generation biosensing. *Trends Biotechnol.* **37**, 730–743 (2019).
11. Li, S. Y. et al. CRISPR-Cas12a-assisted nucleic acid detection. *Cell Discov.* **4**, 20 (2018).
12. Kim, D. et al. Genome-wide analysis reveals specificities of Cpf1 endonucleases in human cells. *Nat. Biotechnol.* **34**, 863–868 (2016).
13. Yan, W. X. et al. BLISS is a versatile and quantitative method for genome-wide profiling of DNA double-strand breaks. *Nat. Commun.* **8**, 15058 (2017).
14. Jones, S. K. Jr et al. Massively parallel kinetic profiling of natural and engineered CRISPR nucleases. *Nat. Biotechnol.* **39**, 84–93 (2021).
15. Schelling, M. A., Nguyen, G. T. & Sashital, D. G. CRISPR-Cas effector specificity and cleavage site determine phage escape outcomes. *PLoS Biol.* **21**, e3002065 (2023).
16. Nguyen, L. T., Smith, B. M. & Jain, P. K. Enhancement of trans-cleavage activity of Cas12a with engineered crRNA enables amplified nucleic acid detection. *Nat. Commun.* **11**, 4906 (2020).
17. Xiao, H. et al. CRISPR techniques and potential for the detection and discrimination of SARS-CoV-2 variants of concern. *Trends Anal. Chem.* **161**, 117000 (2023).
18. Kim, Y. H. et al. Sniper2L is a high-fidelity Cas9 variant with high activity. *Nat. Chem. Biol.* **19**, 972–980 (2023).
19. Bravo, J. P. K. et al. Structural basis for mismatch surveillance by CRISPR-Cas9. *Nature* **603**, 343–347 (2022).
20. Kleinstiver, B. P. et al. Engineered CRISPR-Cas12a variants with increased activities and improved targeting ranges for gene, epigenetic and base editing. *Nat. Biotechnol.* **37**, 276–282 (2019).
21. Dong, C., Gou, Y. & Lian, J. SgRNA engineering for improved genome editing and expanded functional assays. *Curr. Opin. Biotechnol.* **75**, 102697 (2022).
22. Kocak, D. D. et al. Increasing the specificity of CRISPR systems with engineered RNA secondary structures. *Nat. Biotechnol.* **37**, 657–666 (2019).
23. Ke, Y. et al. 2′-O-Methyl modified guide RNA promotes the single nucleotide polymorphism (SNP) discrimination ability of CRISPR-Cas12a systems. *Chem. Sci.* **13**, 2050–2061 (2022).
24. Lee, H. J., Kim, H. J., Park, Y. J. & Lee, S. J. Efficient single-nucleotide microbial genome editing achieved using CRISPR/Cpf1 with maximally 3′-end-truncated crRNAs. *ACS Synth. Biol.* **11**, 2134–2143 (2022).
25. Fu, Y., Sander, J. D., Reyon, D., Cascio, V. M. & Joung, J. K. Improving CRISPR-Cas nuclease specificity using truncated guide RNAs. *Nat. Biotechnol.* **32**, 279–284 (2014).
26. Ooi, K. H. et al. An engineered CRISPR-Cas12a variant and DNA-RNA hybrid guides enable robust and rapid COVID-19 testing. *Nat. Commun.* **12**, 1739 (2021).
27. He, C. et al. Rapid and accurate detection of SARS-CoV-2 mutations using a Cas12a-based sensing platform. *Biosens. Bioelectron.* **198**, 113857 (2022).
28. Huang, X., Zhang, F., Zhu, K., Lin, W. & Ma, W. dsmCRISPR: dual synthetic mismatches CRISPR/Cas12a-based detection of SARS-CoV-2 D614G mutation. *Virus Res*. **304**, 198530 (2021).
29. Ling, C. et al. Two CRISPR/Cas12a-based methods for fast and accurate detection of single-base mutations. *Anal. Chim. Acta* **1247**, 340881 (2023).
30. Zhang, W. et al. PAM-independent ultra-specific activation of CRISPR-Cas12a via sticky-end dsDNA. *Nucleic Acids Res.* **50**, 12674–12688 (2022).
31. Meng, Q. et al. Detection of the SARS-CoV-2 D614G mutation using engineered Cas12a guide RNA. *Biotechnol. J.* **16**, e2100040 (2021).
32. Zhang, W. et al. The off-target effect of CRISPR-Cas12a system toward insertions and deletions between target DNA and crRNA sequences. *Anal. Chem.* **94**, 8596–8604 (2022).
33. Cromwell, C. R. et al. Incorporation of bridged nucleic acids into CRISPR RNAs improves Cas9 endonuclease specificity. *Nat. Commun.* **9**, 1448 (2018).
34. Ryan, D. E. et al. Improving CRISPR-Cas specificity with chemical modifications in single-guide RNAs. *Nucleic Acids Res.* **46**, 792–803 (2018).
35. Chavez, A. et al. Precise Cas9 targeting enables genomic mutation prevention. *Proc. Natl. Acad. Sci. USA* **115**, 3669–3673 (2018).
36. Jeon, Y. et al. Direct observation of DNA target searching and cleavage by CRISPR-Cas12a. *Nat. Commun.* **9**, 2777 (2018).
37. Wang, R. et al. Engineering of the LAMP-CRISPR/Cas12b platform for Chlamydia psittaci detection. *J. Med. Microbiol*. **72**, https://doi.org/10.1099/jmm.0.001781 (2023).
38. Rutkauskas, M. et al. A quantitative model for the dynamics of target recognition and off-target rejection by the CRISPR-Cas Cascade complex. *Nat. Commun.* **13**, 7460 (2022).
39. Li, L. et al. HOLMESv2: a CRISPR-Cas12b-assisted platform for nucleic acid detection and DNA methylation quantitation. *ACS Synth. Biol.* **8**, 2228–2237 (2019).
40. Strohkendl, I., Saifuddin, F. A., Rybarski, J. R., Finkelstein, I. J. & Russell, R. Kinetic basis for DNA target specificity of CRISPR-Cas12a. *Mol. Cell* **71**, 816–824 e813 (2018).
41. Pacesa, M. et al. Structural basis for Cas9 off-target activity. *Cell* **185**, 4067–4081 e4021 (2022).
42. Kimsey, I. J., Petzold, K., Sathyamoorthy, B., Stein, Z. W. & Al-Hashimi, H. M. Visualizing transient Watson-Crick-like mispairs in DNA and RNA duplexes. *Nature* **519**, 315–320 (2015).
43. Wessels, H. H. et al. Prediction of on-target and off-target activity of CRISPR-Cas13d guide RNAs using deep learning. *Nat. Biotechnol.* https://doi.org/10.1038/s41587-023-01830-8 (2023).
44. Bisaria, N., Jarmoskaite, I. & Herschlag, D. Lessons from enzyme kinetics reveal specificity principles for RNA-guided nucleases in RNA interference and CRISPR-based genome editing. *Cell Syst.* **4**, 21–29 (2017).
45. Donohoue, P. D. et al. Conformational control of Cas9 by CRISPR hybrid RNA-DNA guides mitigates off-target activity in T cells. *Mol. Cell* **81**, 3637–3649.e3635 (2021).
46. Eslami-Mossallam, B. et al. A kinetic model predicts SpCas9 activity, improves off-target classification, and reveals the physical basis of targeting fidelity. *Nat. Commun.* **13**, 1367 (2022).
47. Li, S. et al. A one-step, one-pot CRISPR nucleic acid detection platform (CRISPR-top): application for the diagnosis of COVID-19. *Talanta* **233**, 122591 (2021).
48. Yang, J. et al. Rapid SARS-CoV-2 Variants Enzymatic Detection (SAVED) by CRISPR-Cas12a. *Microbiol. Spectr.* **10**, e0326022 (2022).
49. Higgins, M. et al. Characterizing the impact of primer-template mismatches on recombinase polymerase amplification. *J. Mol. Diagn.* **24**, 1207–1216 (2022).
50. Lin, M. et al. Glycerol additive boosts 100-fold sensitivity enhancement for one-pot RPA-CRISPR/Cas12a assay. *Anal. Chem.* **94**, 8277–8284 (2022).
51. Welch, N. L. et al. Multiplexed CRISPR-based microfluidic platform for clinical testing of respiratory viruses and identification of SARS-CoV-2 variants. *Nat. Med.* **28**, 1083–1094 (2022).
52. Jedrzejczyk, D. J. et al. CRISPR-Cas12a nucleases function with structurally engineered crRNAs: SynThetic trAcrRNA. *Sci. Rep.* **12**, 12193 (2022).

53. Zhang, J. P. et al. Different effects of sgRNA length on CRISPR-mediated gene knockout efficiency. *Sci. Rep.* **6**, 28566 (2016).
54. Huang, X. et al. Structural basis for two metal-ion catalysis of DNA cleavage by Cas12i2. *Nat. Commun.* **11**, 5241 (2020).
55. Zhang, B. et al. Mechanistic insights into the R-loop formation and cleavage in CRISPR-Cas12i1. *Nat. Commun.* **12**, 3476 (2021).

## Acknowledgements

This research was funded by The Key Research and Development Project of Jiangsu Province (BE2023694); Jiangsu Provincial Health Commission Project (H2023060); Jiangsu Provincial Association for Science and Technology Youth Talent Support Program (JSTJ-2023-WJ004); Key Laboratory Project of Changzhou City (CM20223016); Leading Talent of Changzhou "The 14th Five-Year Plan" High-Level Health Talents Training Project (2022CZLJ025); Changzhou Science and Technology Plan Project (Grant No. CJ20220114, CE20225041); Young Talent Development Plan of Changzhou Health Commission (CZQM2020113, CZQM202011, CZQM2022023).

## Author contributions

Xujian Mao conceived the project, provided overall supervision, and wrote the manuscript. Jian Xu designed the experiments and performed the experiments and analyzed the data. Jingyi Jiang, Qiong Li, and Ping Yao performed the experiments. Jinyi Jiang and Li Gong assisted with clinical validations. Yin Dong, Bowen Tu, and Rong Wang assisted with the bioinformatics analysis of SARS-CoV-2 genomes. Hongbing Tang, Fang Yao, and Fengming Wang wrote the manuscript and contributed reagents/analysis tools.

## Competing interests

The authors declare that a patent has been filed for enhancing the specificity of the CRISPR system. Applicant: Changzhou Center for Disease Control and Prevention. Inventors: Xujian Mao, Fengming Wang, Jian Xu, Jingyi Jiang, Qiong Li, Ping Yao. Status: Patent pending. Patent Application No. 202410287734.6. The remaining authors declare no competing interests.

## Additional information

**Supplementary information** The online version contains supplementary material available at https://doi.org/10.1038/s42003-024-07173-7.

**Correspondence** and requests for materials should be addressed to Xujian Mao, Hongbing Tang, Fang Yao or Fengming Wang.

**Peer review information** *Communications Biology* thanks Baolei Yuan and the other, anonymous, reviewer for their contribution to the peer review of this work. Primary Handling Editors: Dr Mo Li and Dr Ophelia Bu. A peer review file is available.